ACS OMEGA

http://pubs.acs.org/journal/acsodf

Article

Efficient Synthesis, Spectroscopic Characterization, and Nonlinear Optical Properties of Novel Salicylaldehyde-Based Thiosemicarbazones: Experimental and Theoretical Studies

Saifullah Bullo,[▽] Rifat Jawaria,[▽] Iqra Faiz, Iqra Shafiq, Muhammad Khalid,* Muhammad Adnan Asghar, Rabia Baby, Raha Orfali,* and Shagufta Perveen

Cite This: *ACS Omega* 2023, 8, 13982−13992

Read Online

ACCESS | Metrics & More | Article Recommendations | Supporting Information

ABSTRACT: Currently, we reported the synthesis of six novel salicylaldehyde-based thiosemicarbazones (**BHCT1−HBCT6**) via condensation of salicylaldehyde with respective thiosemicarbazide. Through various spectroscopic methods, UV−visible and NMR, the chemical structures of **BHCT1−HBCT6** compounds were determined. Along with synthesis, a computational study was also performed at the M06/6-31G(d,p) functional. Various analyses such as natural bond orbital (NBO) analysis, natural population analysis, frontier molecular orbital (FMO) analysis, and molecular electrostatic potential surfaces were carried out to understand the nonlinear optical (NLO) characteristics of the synthesized compounds. Additionally, a comparative study was carried out between DFT and experimental results (UV−vis study), and a good agreement was observed in the results. The energy gap calculated through FMOs was found to be in decreasing order as 4.505 (**FHCT2**) > 4.499 (**HBCT6**) > 4.497 (**BHCT1**) = 4.497(**HMCT5**) > 4.386 (**CHCT3**) > 4.241(**AHCT4**) in eV. The global reactivity parameters (GRPs) were attained through E_{HOMO} and E_{LUMO}, which described the stability and hardness of novel compounds. The NBO approach confirmed the charge delocalization and stability of the molecules. Among all the investigated compounds, a larger value (557.085 a.u.) of first hyperpolarizability (β_{tot}) was possessed by **CHCT3**. The NLO response (β_{tot}) of **BHCT1−HBCT6** was found to be 9.145, 9.33, 13.33, 5.43, 5.68, and 10.13 a.u. times larger than that of the standard *para*-nitroaniline molecule. These findings ascertained the potential of entitled ligands as best NLO materials for a variety of applications in modern technology.

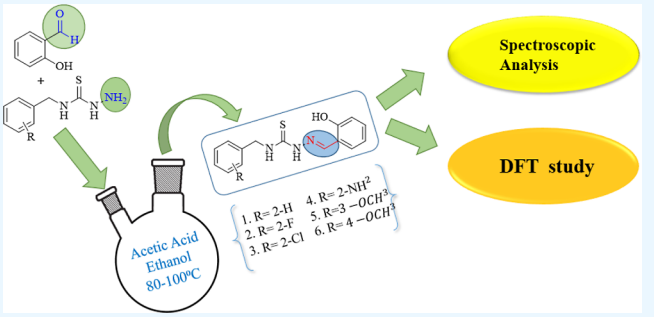

INTRODUCTION

The type of photonic interaction with any matter is regulated by its structure. The primary elements of laser applications and optical systems are optical materials, which are the core subject of current era's scientific research. Nonlinear optical (NLO) materials have gained substantial scientific attention from the time when the first function of laser was discovered.[1,2] The NLO materials are able to alter the incident laser's frequency upon interaction. So far, to improve the NLO response, substantial research has been accomplished on electro-optical materials through various approaches.[3,4] These approaches substantially consist of utilizing molecular systems with extended π-electron structures,[5,6] twisted π-electron structures,[7] the planar donor−π−acceptor (D−π−A) model,[8] octupolar molecules,[9,10] bond length alternation theory,[11] enhanced push−pull properties,[2,12] incorporating metal ligands into the organic compounds, etc.[13] Upon interaction with intense laser light, the NLO substances produce electromagnetic fields of diverse frequencies and phases inducing new applications in holographic imaging, frequency mixing and doubling, telecommunication, optical data storage, and so forth.[14] At present, investigation of short-wavelength NLO crystals together with deep ultraviolet (DUV) and ultraviolet (UV), possessing suitable birefringence, short cutoff edge, and strong second-harmonic generation (SHG) response, is of pronounced interest as suitable birefringence permits phase matching in the short wavelength;[15] a small UV cutoff edge improves the laser damage threshold;[16] and SHG enhances the efficiency of frequency conversion[17] of crystals. Although the aforementioned three factors are mutually regulated,[18] efficient designing of crystals to achieve the abovementioned performance conditions is quiet challenging.

During the past decades, to employ in NLO applications, a diversity of materials have been discovered. Generally, these

Received: January 20, 2023
Accepted: March 21, 2023
Published: April 7, 2023

materials comprise inorganic, organic, organic−inorganic hybrid, and organometallic substances.[19] Lately, numerous experimental and theoretical studies have been accomplished on organic NLO materials owing to their diversity of structures, low economical cost, and easy fabrication.[20] Certain valuable approaches of organic NLO materials are twisted π-electron systems, improved push−pull effects, extended π-electron structures, integration of an alkali metal into the organic complex, and the planar donor−π-conjugated bridge−acceptor (D−π−A) model. Various standard organic materials named push−pull systems consisted of strong donor and acceptor motifs along with a π-conjugated bridge which promotes intramolecular charge transference (ICT) in the compound.[21,22] The ICT comprises a low-energy molecular orbital, obtainable via visible light excitation accountable for molecular polarization. The desired NLO and optical applications are achieved by altering the donor and acceptor motifs or the π-bridge length or the complete molecular arrangement.[23] Heteroatom integration in these organic compounds results in efficient increase in NLO response.[24]

Moreover, thiosemicarbazones (TSCs) showed promising applications in almost every aspect of chemistry; commercially, they are employed in photographic films, dyes, plastic, and textile industry.[25] TSC-based derivatives having donor and acceptor moieties have also gained substantial interest in computational chemistry field and are largely studied by both theoretical and experimental communities. By considering the position of TSCs in biological field and possessing a relative research background in both the synthetic and computational fields,[26,27] here, we have reported the synthesis of salicylaldehyde-based TSC compounds, (*E*)-*N*-benzyl-2-(2-hydroxybenzylidene)hydrazinecarbothioamide (**BHCT1**), (*E*)-*N*-(2-fluorobenzyl)-2-(2-hydroxybenzylidene)-hydrazinecarbothioamide (**FHCT2**), (*E*)-*N*-(2-chlorobenzyl)-2-(2-hydroxybenzylidene)hydrazinecarbothioamide (**CHCT3**), (*E*)-*N*-(2-aminobenzyl)-2-(2-hydroxybenzylidene)hydrazinecarbothioamide (**AHCT4**), (*E*)-2-(2-hydroxybenzylidene)-*N*-(3-methoxybenzyl)-hydrazinecarbothioamide (**HMCT5**), and (*E*)-2-(2-hydroxybenzylidene)-*N*-(4-methoxybenzyl)hydrazinecarbothioamide (**HBCT6**), and then investigated their application in nonlinear optics. To our knowledge, there are no NLO responses accomplished on for-said salicylaldehyde-based TSCs so far. A systematic DFT study along with experimental calculations was carried out to deeply recognize the characteristics of the title molecules. We executed the natural bond orbital (NBO) and NLO analyses of the studied molecules. The UV−visible spectroscopic investigations as well as HOMO and LUMO analyses are adapted to analyze the charge transference process in the chromophore. The GRPs were also calculated to examine the electrophilicity index, electron affinity (EA), ionization potential (IP), softness, hardness, and electron-accepting as well as electron-donating proficiencies of the examined compounds (**BHCT1**−**HBCT6**).

Spectroscopic Data. All novel compounds were characterized as given below.

*(E)-N-Benzyl-2-(2-hydroxybenzylidene) Hydrazinecarbothioamide (**BHCT1**).* Yield, 83%; white amorphous: mp, 201 °C; IR (KBr), (cm^{-1}): 1203 (C═S), 1507 (C═N), 2987 (N−H), 3136 (O−H). UV−vis (ethanol): λ_{max}, = 342 nm. ^{1}H NMR, $^{\delta}$ (ppm): 4.885 (d, 2H, *J* = 8 Hz, CH_2−NCS), 8.444 (s, 1H, OH), 9.009 (t, 1H, *J* = 7.5 Hz, NH−CS), 9.967 (s, 1H, N═CH), 11.661 (s, 1H, CSNHN), 6.810−7.975 (m, 2 phenyl rings). ^{13}CNMR$^{\delta}$ (ppm): 177.964 (C═S), 156.939 (C═N), 44.908 (CH_2−NCS), 116.537, 119.689, 120.823, 127.517, 128.440, 128.768, 129.462, 131.685, 131.843, 136.886 (aromatic C and CH).

*(E)-N-(2-Fluorobenzyl)-2-(2-hydroxybenzylidene) Hydrazinecarbothioamide (**FHCT2**).* Yield, 81%; white amorphous: mp, 214 °C; IR (KBr), (cm^{-1}): 1224 (C═S), 1509 (C═N), 3390, 2994 (N−H), 3134 (O−H). UV−vis (ethanol): λ_{max}, = 340 nm. ^{1}H NMR, $^{\delta}$ (ppm): 4.754 (d, 2H, *J* = 8 Hz, CH_2−NCS), 8.506 (s, 1H, OH), 7.982 (t, 1H, *J* = 10.5 Hz, NH−CS), 10.087 (s, 1H, N═CH), 12.069 (s, 1H, CSNHN), 6.834−7.601 (m, 2 phenyl rings). ^{13}CNMR$^{\delta}$ (ppm): 157.241 (C═S), 138.199 (C═N), 44.908 (CH_2−NCS), 116.592, 119.815, 120.456, 121.473, 121.651, 127.682, 128.946, 129.185, 131.044, 131.436, 132.091, 134.804 (aromatic C and CH).

*(E)-N-(2-Chlorobenzyl)-2-(2-hydroxybenzylidene) Hydrazinecarbothioamide (**CHCT3**).* Yield, 82%; white amorphous: mp, 205 °C; IR (KBr), (cm^{-1}): 1226 (C═S), 1535 (C═N), 2996, 3386 (N−H), 3134 (O−H). UV−vis (ethanol): λ_{max}, = 340 nm. ^{1}H NMR, $^{\delta}$ (ppm): 4.833 (d, 2H, *J* = 8 Hz, CH_2−NCS), 8.408 (s, 1H, OH), 9.007 (t, 1H, *J* = 8 Hz, NH−CS), 9.933 (s, 1H, N═CH), 11.529 (s, 1H, CSNHN), 6.815−7.965 (m, 2 phenyl rings). ^{13}CNMR$^{\delta}$ (ppm): 177.663 (C═S), 156.864 (C═N), 47.020 (CH_2−NCS), 116.503, 118.256, 119.657, 120.865, 127.165, 127.693, 128.622, 131.575, 139.940, 140.018 (aromatic C and CH).

*(E)-N-(2-Aminobenzyl)-2-(2-hydroxybenzylidene) Hydrazinecarbothioamide (**AHCT4**).* Yield, 80%; white amorphous: mp, 180 °C; IR (KBr), (cm^{-1}): 1228 (C═S), 1518 (C═N), 2994, 3384 (N−H), 3134 (O−H). UV−Vis (ethanol): λ_{max}, = 340 nm. ^{1}H NMR, $^{\delta}$ (ppm): 4.963 (d, 2H, *J* = 6.5 Hz, CH_2−NCS), 4.353 (s, 2H, NH_2), 9.935 (s, 1H, OH), 10.364 (s, 1H, NH−CS), 11.615 (s, 1H, N═CH), 12.925 (s, 1H, CSNHN), 6.758−8.941 (m, 2 phenyl rings). ^{13}CNMR$^{\delta}$ (ppm): 176.255 (C═S), 160.665 (C═N), 43.260 (CH_2−NCS), 114.378, 117.113, 117.915, 119.733, 120.073, 120.837, 123.373, 126.445, 128.508, 132.961, 135.725, 156.919 (aromatic C and CH).

*(E)-2-(2-Hydroxybenzylidene)-N-(3-methoxybenzyl) Hydrazinecarbothioamide (**HMCT5**).* Yield, 85%; white amorphous: mp, 210 °C; IR (KBr), (cm^{-1}): 1298 (C═S), 1544 (C═N), 3011, 3304 (N−H), 3396 (O−H). UV−vis (ethanol): λ_{max}, = 341 nm. ^{1}H NMR, $^{\delta}$ (ppm): 4.75 (d, 2H, *J* = 8 Hz, CH_2−NCS), 3.724 (s, 3H, OCH_3), 8.391 (s, 1H, OH), 8.919 (t, 1H, *J* = 7.5 Hz, NH−CS), 9.925 (s, 1H, N═CH), 11.482 (s, 1H, CSNHN), 6.814−7.946 (m, 2 phenyl rings). ^{13}CNMR$^{\delta}$ (ppm): 177.358 (C═S), 158.663 (C═N), 46.354 (CH_2−NCS), 55.522 (OCH_3), 111.399, 114.031, 114.072, 116.465, 116.537, 119.640, 120.880, 125.647, 127.184, 129.163, 131.538, 131.950, 139.785, 156.855 (aromatic C and CH).

*(E)-2-(2-Hydroxybenzylidene)-N-(4-methoxybenzyl) Hydrazinecarbothioamide (**HBCT6**).* Yield, 83%; white amorphous: mp, 203 °C; IR (KBr), (cm^{-1}): 1229 (C═S), 1538 (C═N), 2921, 2999 (N−H), 3391(O−H). UV−vis (ethanol): λ_{max}, = 340 nm. ^{1}H NMR, $^{\delta}$ (ppm): 4.80 (d, 2H, *J* = 7.5 Hz, CH_2−NCS), 3.731 (s, 3H, OCH_3), 8.410 (s, 1H, OH), 8.985 (t, 1H, *J* = 8 Hz, NH−CS), 9.924 (s, 1H, N═CH), 11.535 (s, 1H, CSNHN), 6.798−7.969 (m, 2 phenyl rings). ^{13}CNMR$^{\delta}$ (ppm): 177.817 (C═S), 159.657 (C═N), 46.975 (CH_2−NCS), 55.432 (OCH_3), 112.325, 113.606, 116.512,

https://doi.org/10.1021/acsomega.3c00421
ACS Omega 2023, 8, 13982−13992

119.651, 119.900, 120.868, 127.135, 129.703, 131.575, 139.893, 141.630, 156.876 (aromatic C and CH).

RESULTS AND DISCUSSION

The synthesized TSCs (**BHCT1−HBCT6**) were examined through ^{1}H NMR and ^{13}C NMR. The occurrence of the Schiff base was instantaneously apparent from the NMR spectra. In the ^{1}H NMR spectra of compounds **BHCT1−HBCT6**, the distinctive doublet signal arising from the protons of CH_2−NCS was observed at 4.75−4.963 ppm. The singlet chemical shift of N═CH has appeared at 9.924−11.615 ppm. A significant signal due to NH−CS was observed at 7.982−10.364 ppm. The hydrazinic (CSNHN) functional group showed a singlet peak in the deshielded region at 11.482−12.925 ppm. The hydroxyl protons displayed a singlet peak at 8.391−9.935 ppm in compounds **BHCT1−HBCT6**. In **AHCT4**, the singlet chemical shift in the shielded region at 4.353 ppm was attributed to the NH_2 proton. The peaks appearing at 3.724 and 3.731 ppm in compounds **HMCT5** and **HBCT6**, respectively, corresponded to OCH_3 protons. The multiplet signals due to aromatic protons in **BHCT1−HBCT6** were noticed in the region at 6.758−8.941 ppm. In the ^{13}C NMR spectra, the signal appeared at 138.199−160.665 ppm was allocated to the C═N azomethine functionality. The existence of the C═S signal was observed at 157.241−177.964 ppm, while the carbon of CH_2−NCS showed an upfield peak at 43.260−47.020 ppm. The signals of aromatic carbons were noticed at 111.399−156.919 ppm (Figures S7−S17).

NBO Analysis. The clear and comprehensive assessment of the molecular phenomena such as conjugation, interactions between bonds, intra- and intermolecular hydrogen bonding, hyperconjugative interactions, and movement of charge in electron-deficient and electron-rich groups is accomplished by NBO analysis.[28,29] Additionally, NBO analysis assists to explicate the relocation of charges from a filled donor to an empty acceptor in donor−π−acceptor configurations.[30] Herein, second-order perturbation theory is adapted to depict the energy of stabilization, related to interactions of donor−acceptor.[29] In this examination, NBO (i) symbolizes the donor orbital and NBO (j) denotes the acceptor orbital and the energy of stabilization as the resonance of electron is denoted by $E^{(2)}$, which could be calculated through eq 1.

$$E^{(2)} = q_i \frac{(F_{i,j})^2}{\varepsilon_j - \varepsilon_i} \quad (1)$$

Although q_i represents the orbital occupancy, ε_i symbolizes the diagonal NBO Fock matrix elements and $F_{i,j}$ denotes the off-diagonal NBO Fock matrix elements.[31] Some selected values of NBOs for compounds **BHCT1−HBCT6** are listed in Table 1, while Tables S1−S6 demonstrated certain more transitions representing established conjugation. The structures with labeled atoms are shown in Figure S18.

Mostly, four types of transitions, namely, $\sigma \rightarrow \sigma^*$, $\pi \rightarrow \pi^*$, LP $\rightarrow \sigma^*$, and LP $\rightarrow \pi^*$, are perceived for the studied chromophores. Among these, $\sigma \rightarrow \sigma^*$ transitions possess smaller magnitude and are least dominant, while $\pi \rightarrow \pi^*$ are most prominent having larger values. The electronic transitions involving LP $\rightarrow \sigma^*$ and LP $\rightarrow \pi^*$ are intermediate types of transitions. The favorable transitions observed are π(C24−C26) $\rightarrow \pi^*$(C25−C27), π(C23−C25) $\rightarrow \pi^*$(C24−C26), π(C4−C5) $\rightarrow \pi^*$(C2−C3), π(C23−C25) $\rightarrow \pi^*$(C24−C26), π(C2−C3) $\rightarrow \pi^*$(C1−C6), and π(C23−C25) $\rightarrow \pi^*$(C24−C26) having largest values of stabilization energies 23.73, 23.73, 24.48, 23.68, 24.50, and 23.73 kcal/mol in molecules **BHCT1−HBCT6**, respectively, representing the existence of conjugation (Table 1). In contrast, least stabilization energies, 6.81, 6.85, 6.14, 6.96, 6.81, and 6.80 kcal/mol, indicate the conjugation in π(N21−C22) $\rightarrow \pi^*$(C24−C26), π(N20−C21) $\rightarrow \pi^*$(C23−C25), π(N20−C21) $\rightarrow \pi^*$(C23−C24), π(N20−C21) $\rightarrow \pi^*$(C23−C25), π(N20−C21) $\rightarrow \pi^*$(C23−C25), and π(N20−C21) $\rightarrow \pi^*$(C23−C25) transitions, respectively (Table 1). The $\sigma \rightarrow \sigma^*$ transitions such as σ(C22−C24) $\rightarrow \sigma^*$(N19−N21), σ(C21−C23) $\rightarrow \sigma^*$(N18−N20), σ(C21−C23) $\rightarrow \sigma^*$(N18−N20), σ(C21−C23) $\rightarrow \sigma^*$(N18−N20), σ(C21−C23) $\rightarrow \sigma^*$(N18−N20), and σ(C21−C23) $\rightarrow \sigma^*$(N18−N20) are found with greater values of stabilization energies like 5.66, 5.65, 5.66, 5.61, 5.66, and 5.67 kcal/mol for **BHCT1−HBCT6**, respectively. Furthermore, the least values of energies associated with $\sigma \rightarrow \sigma^*$ at 0.78, 0.52, 0.55, 0.53, 0.56, and 0.53 kcal/mol are associated with σ(C27−H31) $\rightarrow \sigma^*$(C25−O34), σ(C3−C11) $\rightarrow \sigma^*$(C11−H13), σ(C3−C11) $\rightarrow \sigma^*$(C11−H13), σ(C1−C6) $\rightarrow \sigma^*$(C2−N35), σ(C3−C11) $\rightarrow \sigma^*$(C11−H13), and σ(C11−N14) $\rightarrow \sigma^*$(N14−C16) of **BHCT1−HBCT6**, respectively. The values of stabilization

Table 1. NBO Investigation of the Mentioned Molecules BHCT1−HBCT6

compounds	donor (i)	type	acceptor (j)	type	$E^{(2)a}$ [kcal/mol]
BHCT1	C24−C26	π	C25−C27	π^*	23.73
	N21−C22	π	C24−C26	π^*	6.81
	C22−C24	σ	N19−N21	σ^*	5.66
	C27−H31	σ	C25−O34	σ^*	0.78
	O34	LP(2)	C25−C27	π^*	19.62
	N15	LP(1)	C2−H8	σ^*	0.56
FHCT2	C23−C25	π	C24−C26	π^*	23.73
	N20−C21	π	C23−C25	π^*	6.85
	C21−C23	σ	N18−N20	σ^*	5.65
	C3−C11	σ	C11−H13	σ^*	0.52
	F35	LP(3)	C1−C2	π^*	20.66
	N20	LP(1)	N14−C16	σ^*	0.60
CHCT3	C4−C5	π	C2−C3	π^*	24.48
	N20−C21	π	C23−C23	π^*	6.14
	C21−C23	σ	N18−N20	σ^*	5.66
	C3−C11	σ	C11−H13	σ^*	0.55
	O33	LP(2)	C23−C24	π^*	19.37
	N20	LP(1)	N14−C16	σ^*	0.60
AHCT4	C23−C25	π	C24−C26	π^*	23.68
	N20−C21	π	C23−C25	π^*	6.96
	C21−C23	σ	N18−N20	σ^*	5.61
	C1−C6	σ	C2−N35	σ^*	0.53
	O33	LP(2)	C24−C26	π^*	19.65
	N20	LP(1)	N14−C16	σ^*	0.59
HMCT5	C2−C3	π	C1−C6	π^*	24.50
	N20−C21	π	C23−C25	π^*	6.81
	C21−C23	σ	N18−N20	σ^*	5.66
	C3−C11	σ	C11−H13	σ^*	0.56
	O33	LP(2)	C24−C26	π^*	19.63
	N14	LP(1)	C2−H7	σ^*	0.57
HBCT6	C23−C25	π	C24−C26	π^*	23.73
	N20−C21	π	C23−C25	π^*	6.80
	C21−C23	σ	N18−N20	σ^*	5.67
	C11−N14	σ	N14−C16	σ^*	0.53
	O33	LP(2)	C24−C26	π^*	19.62
	N14	LP(1)	C2−H8	σ^*	0.57

https://doi.org/10.1021/acsomega.3c00421
ACS Omega 2023, 8, 13982−13992

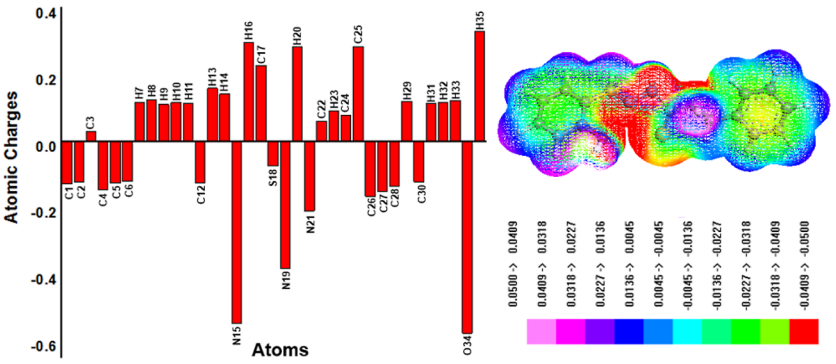

BHCT1

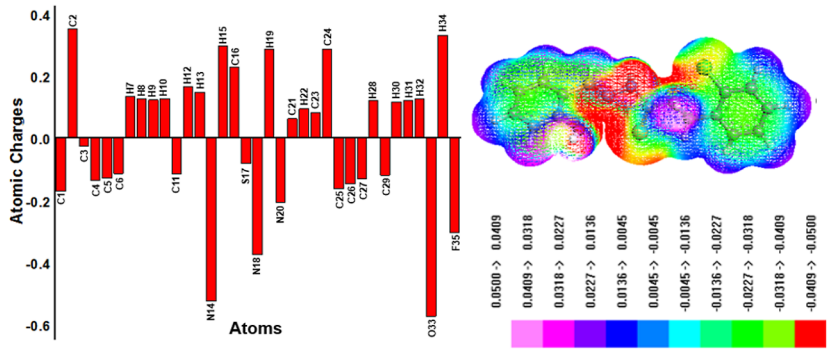

FHCT2

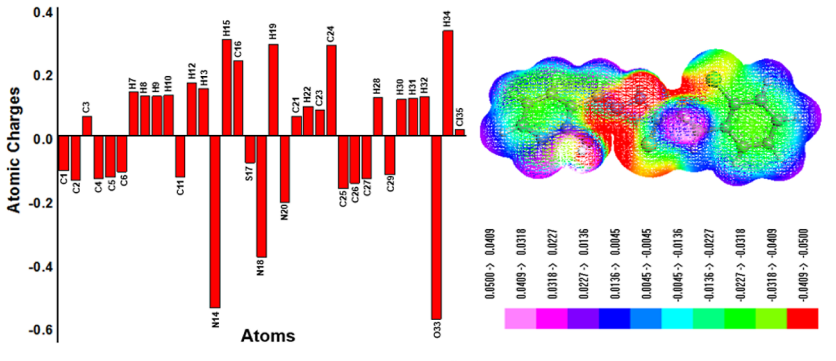

CHCT3

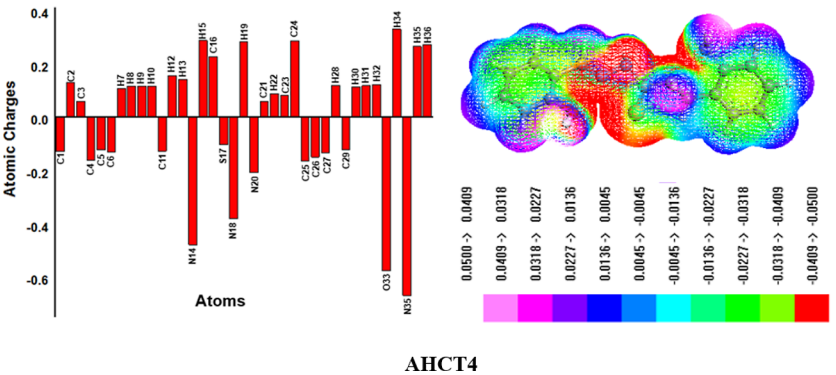

AHCT4

Figure 1. continued

https://doi.org/10.1021/acsomega.3c00421
ACS Omega 2023, 8, 13982−13992

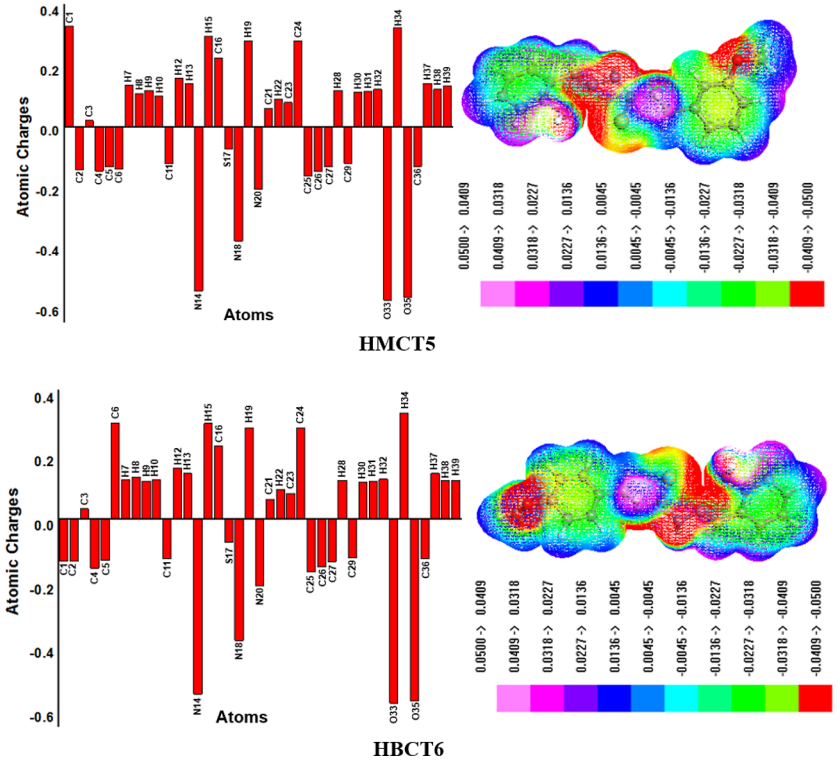

Figure 1. Graphical representation of NPA and MEP maps of **BHCT1−HBCT6**.

energy accompanying with $\sigma \rightarrow \sigma^*$ transitions are detected to be weaker than those accompanying with $\pi \rightarrow \pi^*$ transitions due to very poor transitions between donors and acceptors. Moreover, in the instance of resonance, the transitions such as LP2(O34) → π^*(C25−C27), LP3(F35) → π^*(C1−C2), LP2(O33) → π^*(C23−C24), LP2(O33) → π^*(C24−C26), LP2(O33) → π^*(C24−C26), and LP2(O33) → π^*(C24−C26) are noticed which afford the stabilization energies of 19.62, 20.66, 19.37, 19.65, 19.63, and 19.62 kcal/mol in **BHCT1−HBCT6**, respectively. In **BHCT1−HBCT6** molecules, the other lone pair transitions such as LP1(N15) → σ^*(C2−H8), LP1(N20) → σ^*(N14−C16), LP1(N20) → σ^*(N14−C16), LP1(N20) → σ^*(N14−C16), LP1(N14) → σ^*(C2−H7), and LP1(N14) → σ^*(C2−H8) are also seen with minor stabilization energies of 0.56, 0.60, 0.60, 0.59, 0.57, and 0.57 kcal/mol, respectively. From the earlier discussion, it seems that **CHCT3** and **HMCT5** exhibited the highest stability because of prolonged hyperconjugation with 24.48 and 24.50 kcal/mol stabilization energy values. However, extended conjugation, strong hyperconjugative interactions, and internal charge shifting exist in all the studied compounds, which lead to the stability of said compounds and offer an indication as to the red shift behavior of these compounds, giving them exclusive NLO features.

Natural Population Analysis and Molecular Electrostatic Potential Analysis. The phenomenon associates with the electronegativity equalization, the electrostatic potential (EP) on the outer surfaces, and the process of atomic charge transformation in reactions can be elucidated by natural population analysis (NPA).[32] The electronic charges of molecules have substantial involvement in the bonding capability and molecular conformation.[33] To understand the applications of a chemical system, NPA is very helpful to compute the atomic charges in depth. Similarly, molecular electrostatic potential (MEP) elucidates the positive, negative, and neutral EP through the assistance of a color band.[34] MEP is a scheme of constant electron density surface and EP, which is utilized to localize the electron acceptor and donor faces for the nucleophilic and electrophilic attack, respectively. It explains the correlation between molecular structures and physicochemical properties.[35] The red color indicates the probability of the electrophilic attack, while the green and blue colors show the probability of the nucleophilic attack in MEP.[36] The extent of EP decreases in the following order: red < orange < yellow < green < blue.[37] The NPA and MEP **BHCT1−HBCT6** were examined by utilizing the M06 level of theory with the 6-31G(d,p) basis set, and their pictographs are shown in Figure 1. The Mulliken population data exposed that the electronegative atoms such as N, S, O, and F in the entitled ligands **BHCT1−HBCT6** generate an uneven redistribution of electron density on the aromatic rings. The oxygen and nitrogen atoms of molecules exhibited negative values, while all the hydrogen atoms displayed positive values. Further, MEP maps also support the NPA data as the red portions in MEP graphs show the presence of most electronegative sulfur, oxygen, and nitrogen atoms which are the most appropriate sites for the electrophilic attack in **BHCT1−HBCT6**. In all the investigated compounds, the charge distribution reflects that the carbon atoms attached with electronegative oxygen, nitrogen, and sulfur atoms contain positive charges. Conversely, the blue color is frequently confined over carbon atoms which are located near the electronegative atoms, signifying that C atoms are prone to the nucleophile attack in **BHCT1−HBCT6**, whereas the rest of the part of molecules suggest attaining almost neutrality concerning EP. Similarly, in **FHCT2**, the carbon atom attached with fluorine also possessed a positive charge. On the other hand, the nitrogen, sulfur, oxygen, and fluorine atoms attached with carbon atoms hold a

https://doi.org/10.1021/acsomega.3c00421
ACS Omega 2023, 8, 13982−13992

Table 2. Energies of HOMO/LUMO along with $\Delta E = E_{LUMO} - E_{HOMO}$ in eV of BHCT1−HBCT6 Compounds[a]

	BHCT1		FHCT2		CHCT3		AHCT4		HMCT5		HBCT6	
MOs	*E*	Δ*E*	*E*	Δ*E*	*E*	Δ*E*	*E*	Δ*E*	*E*	Δ*E*	*E*	Δ*E*
HOMO	−5.959	4.497	−5.897	4.505	−5.804	4.386	−5.410	4.241	−5.956	4.497	−5.992	4.499
LUMO	−1.462		−1.392		−1.418		−1.169		−1.459		−1.493	

[a]*E* = energy, MOs = molecular orbitals.

negative charge. The exceptional behavior is observed in compound **CHCT3**, where the Cl atom that attaches with carbon possesses a slightly positive charge as well as blue color, which might be due to the geometric effect. The other carbon atoms in **BHCT1−HBCT6** comprise a negative charge because they are bonded with comparatively more electropositive hydrogen atoms. All hydrogen atoms also possessed positive charges.

UV−Vis Analysis. To examine the absorption phenomenon, charge transference properties, and excitations of molecular orbital in **BHCT1−HBCT6**, UV−vis spectral analysis has been accomplished at the same functional of TD-DFT. The comparative results of theoretical and experimental λ_{max} along with the oscillator strength (f_{os}), transition energy, and nature of molecular orbital excitations for inspected molecules (**BHCT1−HBCT6**) are presented in Table S7, while their spectra are shown in Figures S1−S6. All of the compounds display absorbance in the ultraviolet region. Computed absorption wavelengths are recorded to be 236−334, 239−333, and 245−332 nm for **BHCT1−CHCT3**, respectively, which show reasonable agreement with the experimental absorption wavelengths: 342, 340, and 340 nm. In the same way, TD-DFT-based absorption wavelengths for **AHCT4−HBCT6** are noticed at 262−339, 253−334, and 254−335 nm, respectively, which are in accordance with the experimentally obtained values: 340, 341, and 340 nm. This closely related correspondence endorses that the designated computational approach is apposite enough. Among all the synthesized compounds, the simulated maximum absorption spectrum is investigated in compound **AHCT4** (λ_{max} = 339 nm) with lower excitation energy (3.650 eV), which shows that this compound could possess significant NLO properties.

Frontier Molecular Orbitals. The frontier molecular orbitals (FMOs) (LUMO and HOMO) are widely employed by chemists and physicists to unveil the reactivity of molecules, their optoelectronic properties, and the ability to absorb light.[27,38] Furthermore, other perspectives including molecular interactions, charge transfer, chemical stability, and UV−Vis spectra are also described through the assistance of FMOs.[39,40] Materials having less energy gap ($\Delta E = E_{LUMO} - E_{HOMO}$) have been considered as soft with high chemical reactivity and less kinetic stability with a greater probability of intramolecular charge transfer (ICT) and vice versa.[39,41] The FMO study was accomplished at the TD-DFT/M06/6-31G(d,p) functional to estimate the energies of HOMO and LUMO along with their band gap ($\Delta E = E_{LUMO} - E_{HOMO}$) for compounds **BHCT1−HBCT6**. The outcomes are tabularized in Table 2, and the pictorial description is presented in Figure 2. Moreover, the higher orbital values like HOMO − 1/LUMO + 1 and HOMO − 2/LUMO − 2 for these synthesized chromophores can be seen in Table S14.

Table 2 reveals that all the compounds showed a comparable value of energy gap; nevertheless, **AHCT4** possesses a lower (4.241 eV) and **FHCT2** possesses a higher (4.505 eV) band gap among **BHCT1−HBCT6** compounds. The reduction in

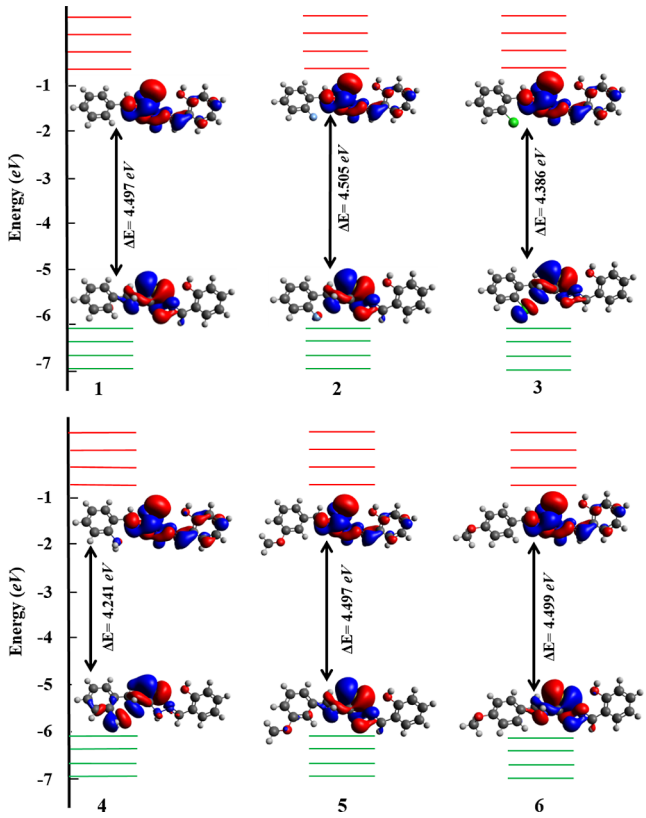

Figure 2. Frontier molecular orbitals of **BHCT1−HBCT6** chromophores.

energy band gap in **AHCT4** occurs owing to the presence of the electron-donating amine ($-NH_2$) moiety, which enhances the electron density over the benzene ring, which in turn creates an excellent push−pull effect. The overall band gap for **BHCT1−HBCT6** is measured to be 4.497, 4.505, 4.386, 4.241, 4.497, and 4.499 eV, respectively. This Δ*E* value between the orbitals of LUMO and HOMO for compounds (**BHCT1−HBCT6**) is detected to be approximately equivalent in magnitude. The larger Δ*E* value showed that all the investigated compounds possess low reactivity and high stability. In summary, among all **BHCT1−HBCT6** compounds, **AHCT4** with lower energy gap and greater bathochromic shift along with significant stabilization energy due to resonance and strong electron-withdrawing units could be an efficient NLO material.

Besides the energies, the FMO analysis also shows that the ICT from HOMO toward LUMO occurs through HOMO → LUMO transition. In compounds **BHCT1−CHCT3**, the charge density in HOMO is located on 2-methylenehydrazinecarbothioamide, *N*-(3-fluoropropyl)-2-methylenehydrazinecarbothioamide, and *N*-(3-chloropropyl)-2-methylenehydrazinecarbothioamide, respectively. For LUMO, the charge cloud is concentrated on (*E*)-2-(2-hydroxybenzylidene) hydrazine-

https://doi.org/10.1021/acsomega.3c00421
ACS Omega 2023, 8, 13982−13992

Table 3. Global Reactivity Parameters of BHCT1−HBCT6, in eV

compounds	IP	EA	X	η	μ	ω	σ
BHCT1	5.959	1.462	3.710	2.248	−3.710	3.061	0.222
FHCT2	5.897	1.392	3.644	2.252	−3.644	2.948	0.221
CHCT3	5.804	1.418	3.611	2.193	−3.611	2.972	0.227
AHCT4	5.410	1.169	3.289	2.120	−3.289	2.551	0.235
HMCT5	5.956	1.459	3.707	2.248	−3.707	3.056	0.222
HBCT6	5.992	1.493	3.742	2.249	−3.742	3.113	0.222

carbothioamide for compounds **BHCT1−CHCT3**. Furthermore, the HOMO charge density of **AHCT4** is accumulated on *N*-(3-amino-2-methylenebut-3-en-1-yl)-2-methylenehydrazinecarbothioamide, while for **HMCT5** and **HBCT6**, it is located on *N*-methyl-2-methylenehydrazinecarbothioamide, while, in the case of LUMO, the charge density is particularly spread on (*E*)-2-(2-hydroxybenzylidene) hydrazinecarbothioamide for compounds **AHCT4−HBCT6**. This proves the proficient charge transference from donor to acceptor via the π-conjugated bridge in all studied compounds, which recommended that these molecules would have exceptional applications as NLO materials.

Global Reactivity Parameters. The global electrophilicity index (ω), IP, global hardness (η), electronegativity (X), global softness (σ), chemical potential (μ), and EA have been estimated as global reactivity descriptors. GRPs are recognized as very proficient parameters for optoelectronic applications and biological activity.[42,43] The energies of LUMO and HOMO are an important factor in determining the global reactivity descriptors. Typically, the molecule possessing high energy difference is considered as stable, nonreactive, and hard species and vice versa.[43,44] GRPs are estimated by utilizing eqs 2−8,[30,33,43,45] which are mentioned below

$$\mathrm{IP} = -E_{\mathrm{HOMO}} \tag{2}$$

$$\mathrm{EA} = -E_{\mathrm{LUMO}} \tag{3}$$

$$\mu = -\frac{(\mathrm{IP} + \mathrm{EA})}{2} \tag{4}$$

$$X = \frac{[\mathrm{IP} + \mathrm{EA}]}{2} \tag{5}$$

$$\eta = \frac{(\mathrm{IP} - \mathrm{EA})}{2} \tag{6}$$

$$\sigma = \frac{1}{(\mathrm{IP} - \mathrm{EA})} \tag{7}$$

$$\omega = \frac{\mu^2}{2\eta} \tag{8}$$

Table 3 shows that the larger IP values are noticed in comparison to EA values unfolding the enhanced competency of the accepting electron of the studied molecules. The values of EA and IP for **BHCT1**, **HMCT5**, and **HBCT6** are noticed to be larger than those for **FHCT2**, **CHCT3**, and **AHCT4**. The chemical hardness values for **BHCT1−HBCT6** are observed to be larger than their chemical softness values. The larger values of hardness demonstrate more stability and less reactivity of **BHCT1−HBCT6**. The value of chemical hardness is larger for **FHCT2** (2.252 eV) as compared to others, which indicates its high stability. The reactivity and stability of molecules also associated with the chemical potential. The chemical potential (μ) order in **BHCT1−HBCT6** in eV is as follows: (**AHCT4** = −3.289 eV) < (**CHCT3** = −3.611 eV) < (**FHCT2** = −3.644 eV) < (**HMCT5** = −3.707 eV) < (**BHCT1** = −3.710 eV) < (**HBCT6** = −3.742 eV). The above-mentioned results have shown the greater stability and less reactivity of all the investigated molecules.

NLO Properties. Recently, the NLO response of organic compounds has set off the fascinated subject of discussion in numerous fields.[46] NLO compounds are extensively used in electrochemical sensors, data storage devices, optical memory devices, optical switches, luminescent materials, signal processing, communication technology, micro-fabrication, and medicinal drugs.[47] Organic materials are highly capable of displaying strong NLO response[48] because of asymmetric polarization. The mechanism of ICT is associated with electron-withdrawing or electron-donating moieties since these types of responses are linked with a conjugated system of π-framework.[49,50] By considering the average linear polarizability $\langle\alpha\rangle$ and first hyperpolarizability (β_{tot}), association to the structural and NLO properties is illustrated by quantum chemical calculations (DFT).[51,52] Generally, first hyperpolarizability (β_{tot}) is a function of the NLO response because of the strong ICT that occurred via the π-bridge system.[53] The NLO analysis using M06/6-31G(d,p) was performed to accomplish the ICT characteristics which are accountable for the NLO behavior of molecules. The dipole moment (μ),[54] the average linear polarizability $\langle\alpha\rangle$,[55] and the first hyperpolarizability (β)[56] values are calculated through the following equations. Additionally, a comparative study is also developed between the *para*-nitroaniline (*p*-NA), which is regarded as a prototype NLO material, and because of the presence of strong donor (amino) and acceptor (nitro) groups, significant NLO properties were seen.[57]

$$\mu = (\mu_x^2 + \mu_y^2 + \mu_z^2)^{1/2} \tag{9}$$

$$\langle\alpha\rangle = (a_{xx} + a_{yy} + a_{zz})/3 \tag{10}$$

$$\beta_{\mathrm{tot}} = (\beta_x^2 + \beta_y^2 + \beta_z^2)^{1/2} \tag{11}$$

where $\beta_x = \beta_{xxx} + \beta_{xyy} + \beta_{xzz}$; $\beta_y = \beta_{yxx} + \beta_{yyy} + \beta_{yzz}$; and $\beta_z = \beta_{zxx} + \beta_{zyy} + \beta_{zzz}$.

Some major values of **BHCT1−HBCT6** compounds are shown in Table 4, while their contributing tensors are displayed in Tables S15−S17.

The results of the dipole moment (μ), average linear polarizability $\langle\alpha\rangle$, and first hyperpolarizability (β_{tot}) of **BHCT1−HBCT6** are tabulated in Table 4. The dipole moment is a significant aspect that denotes the interaction between atoms. The overall μ for all the molecules (**BHCT1−HBCT6**) is noticed to be 4.578, 4.899, 5.095, 3.969, 5.247, and 5.251 D, respectively. The relative study of dipole moment among **BHCT1−HBCT6** displays the highest value for

https://doi.org/10.1021/acsomega.3c00421
ACS Omega 2023, 8, 13982−13992

Table 4. Evaluated Values of Dipole Moment (μ), Average Linear polarizability $\langle\alpha\rangle$, and First Hyperpolarizability (β_{tot})[a]

compounds	μ	$\langle\alpha\rangle$	β_{tot}
BHCT1	4.578	223.063	382.199
FHCT2	4.899	222.362	389.840
CHCT3	5.095	233.122	557.085
AHCT4	3.969	233.005	226.855
HMCT5	5.247	240.871	237.257
HBCT6	5.251	242.200	423.362
***p*-NA**	4.9662	79.5	41.7887

[a]Unit for μ_{tot} is Debye (D) and $\langle\alpha\rangle$ and β_{tot} are in a.u.

compound **HBCT6** (5.251 D) and lowest value for **AHCT4** (3.969 D), which displayed the lesser polarity in **AHCT4** than that of others. On relating results with the *p*-NA molecule (4.9662 D), which is utilized here as a standard compound due to its significant NLO properties,[57] all the entitled molecules display 0.92, 0.99, 1.03, 0.80, 1.06, and 1.06 D, greater values of dipole moment than *p*-NA, respectively. The overall dipole moment values decreased in the following order: **BHCT1−HBCT6** as: **HBCT6** > **HMCT5** > **CHCT3** > **FHCT2** > **BHCT1** > **AHCT4**.

The linear response features are described by average linear polarizability $\langle\alpha\rangle$. The average linear polarizability $\langle\alpha\rangle$ with its respective tensor constituents is computed, and the values in a.u. are recorded in Table S16. In the instance of average linear polarizability $\langle\alpha\rangle$, the results are found to be 233.063, 222.362, 233.122, 233.005, 240.871, and 242.200 a.u. in **BHCT1−HBCT6**, respectively, which are near to be equal in magnitude, possessing the largest value in **HBCT6** (242.200 a.u.) and the lowest value in **FHCT2** (222.362 a.u.). The NLO behavior of the molecules is described by β_{tot}. The first hyperpolarizability along with its tensor components is calculated by using a similar level of DFT and basis set for compounds **BHCT1−HBCT6**, and the respective values are recorded in Table S17. Moreover, β_{tot} for **CHCT3** showed a larger value (557.085 a.u.), while **AHCT4** showed a smaller value (226.855 a.u.) among others. The β_{tot} values of compounds **BHCT1−HBCT6** are obtained as 328.199, 387.840, 557.085, 226.855, 237.257, and 423.362 a.u., respectively. Furthermore, the β_{tot} values of all molecules are found to be 9.145, 9.33, 13.33, 5.43, 5.68, and 10.13 a.u. times greater than the standard *p*-NA molecule (β_{tot} = 41.8 a.u.) as shown in Table S17. The descending order of β_{tot} for all the examined molecules is found to be **CHCT3** > **HBCT6** > **FHCT2** > **BHCT1** > **HMCT5** > **AHCT4**. Earlier discussion supports the remarkable NLO response of all the studied molecules.

CONCLUSIONS

Six novel salicylaldehyde-based TSCs were prepared and characterized spectroscopically. Comparative experimental and DFT analyses were executed between UV−vis values for **BHCT1−HBCT6**, and all the experimental results appeared in line with subsequent DFT measurements. The NBO probe demonstrated the successful process of intermolecular charge transfer in the title compounds. Excitingly, the NBO analysis showed that **HMCT5** exhibited greater stability with 24.50 kcal/mol value of stabilization energy. The blue and red colors in MEP diagrams demonstrated that C and H atoms are potential sites for the nucleophilic attack, while N and O atoms are susceptible to the electrophilic attack, which were further supported by Mulliken charges. The $E_{LUMO}-E_{HOMO}$ energy gaps in **BHCT1−HBCT6** were found to be 4.497, 4.505, 4.386, 4.241, 4.497, and 4.499 eV, respectively. The collected data revealed the lower energy gap of **AHCT4**, demonstrating a strong capability of internal charge transfer (ICT). GRPs suggested the chemical stability and hardness of newly synthesized compounds. Furthermore, the NLO study unveiled that the first hyperpolarizability (β_{tot}) values of **BHCT1−HBCT6** were found to be 9.145, 9.33, 13.33, 5.43, 5.68, and 10.13 a.u. times greater than the standard ***p*-NA** molecule (β_{tot} = 41.8 a.u.). However, among all the studied molecules, **CHCT3** showed a larger value (557.085 *a.u.*) of first hyperpolarizability; therefore, it can be summarized that the presently investigated compounds play a notable contribution in the NLO field and might be operated as best NLO compounds in modern technology.

MATERIALS AND METHODS

All the analytical grade compounds were used and obtained from Merck in pure form, and solvents were purchased from chemical suppliers. Both chemicals and solvents were utilized without additional treatment and purification. To take melting points, a Stuart SMP 10 melting point device was employed. A BK D50 UV−vis spectrophotometer with 190−1100 range was used to record electronic spectra. A FTIR Spectrophotometer Tensor 27 was used for FTIR analysis. To record proton and carbon NMR spectra, a Bruker AM 300 spectrometer was used with TMS as an internal standard and DMSO as a solvent. The reaction completion was confirmed through thin-layer chromatography (TLC) by utilizing silica gel-coated aluminum plates (0.5 mm thick; Merck, Darmstadt, Germany), and the spots were imagined under the UV light at 254 *mm*.

Synthesis of TSCs. TSCs were synthesized from substituted thiosemicarbazide by reacting with salicylaldehyde in ethanol. Substituted thiosemicarbazide (0.1 mol) and salicylaldehyde (0.1 mol) were added in a round-bottom flask having ethanol (5 mL), and acetic acid (two to three drops) was added in a dropwise manner. Then, the prepared

Scheme 1. Schematic Representation of Syntheses of Salicylaldehyde-Based TSC Derivatives (BHCT1−HBCT6)

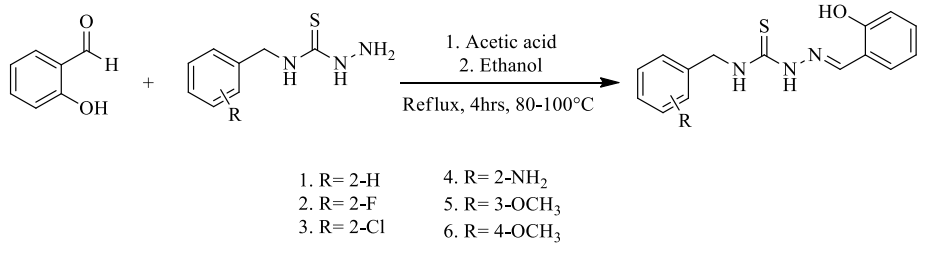

https://doi.org/10.1021/acsomega.3c00421
ACS Omega 2023, 8, 13982−13992

mixture was heated and refluxed at 80−100 °C for 3−4 h. The progression of the reaction was examined periodically through TLC. The schematic route of synthesis compounds can be seen in Scheme 1. On the accomplishment of the reaction, confirmed by TLC, the product was then strained and washed two to three times with ethanol, dried, and collected. The new products were inspected by spectroscopic approaches: UV−vis, IR, and NMR.

Computational Studies. The quantum chemical computational calculations for entitled molecules were accompanied through the Gaussian 09 program package[58] at the M06/6-31G(d,p) level of DFT[59] to inspect the optimized structures and key electronic properties. The absence of imaginary frequency indicated the successful optimization of structures as shown in Tables S8−S13. Additionally, a UV−vis study and frontier molecular orbital (FMO) explorations were achieved via TD-DFT[60] calculations at the stated level of theory and basis set. HOMO−LUMO energy band gaps were additionally employed to inspect the GRPs. Various types of software, Avogadro,[61] Gauss View 6.0,[62] Chemcraft,[63] and Gauss Sum,[64] were utilized to accomplish the FMO, MEP, visualization of optimized geometries, NPA, NBO, and UV−vis analyses.

■ ASSOCIATED CONTENT

Supporting Information

The Supporting Information is available free of charge at https://pubs.acs.org/doi/10.1021/acsomega.3c00421.

NBO, UV−vis data (wave length, excitation energies, and oscillator strengths), FMO, and NLO of reported chromophores were calculated using the M06/6-31G (d,p) method (PDF)

■ AUTHOR INFORMATION

Corresponding Authors

Muhammad Khalid − *Institute of Chemistry, Khwaja Fareed University of Engineering & Information Technology, Rahim Yar Khan 64200, Pakistan; Center for Theoretical and Computational Research, Khwaja Fareed University of Engineering & Information Technology, Rahim Yar Khan 64200, Pakistan;* orcid.org/0000-0002-1899-5689; Email: muhammad.khalid@kfueit.edu.pk, Khalid@iq.usp.br

Raha Orfali − *Department of Pharmacognosy, Collage of Pharmacy, King Saud University, Riyadh 11451, Saudi Arabia*; Email: rorfali@ksu.edu.sa

Authors

Saifullah Bullo − *Department of Human and Rehabilitation Sciences, Begum Nusrat Bhutto Women University, Sukkur Sindh 65170, Pakistan*

Rifat Jawaria − *Institute of Chemistry, Khwaja Fareed University of Engineering & Information Technology, Rahim Yar Khan 64200, Pakistan; Center for Theoretical and Computational Research, Khwaja Fareed University of Engineering & Information Technology, Rahim Yar Khan 64200, Pakistan*

Iqra Faiz − *Institute of Chemistry, Khwaja Fareed University of Engineering & Information Technology, Rahim Yar Khan 64200, Pakistan; Center for Theoretical and Computational Research, Khwaja Fareed University of Engineering & Information Technology, Rahim Yar Khan 64200, Pakistan*

Iqra Shafiq − *Institute of Chemistry, Khwaja Fareed University of Engineering & Information Technology, Rahim Yar Khan 64200, Pakistan; Center for Theoretical and Computational Research, Khwaja Fareed University of Engineering & Information Technology, Rahim Yar Khan 64200, Pakistan*

Muhammad Adnan Asghar − *Department of Chemistry, Division of Science and Technology, University of Education Lahore, Punjab 54770, Pakistan*

Rabia Baby − *Department of Education, Sukkur IBA University, Sukkur 65200, Pakistan*

Shagufta Perveen − *Department of Chemistry, School of Computer, Mathematical and Natural Sciences, Morgan State University, Baltimore, Maryland 21251, United States*

Complete contact information is available at: https://pubs.acs.org/10.1021/acsomega.3c00421

Author Contributions

▽S.B. and R.J. contributed equally.

Notes

The authors declare no competing financial interest.

■ ACKNOWLEDGMENTS

The authors extend their appreciation to the Researcher Supporting Project number (RSP2023R431), King Saud University, Riyadh, Saudi Arabia, for funding this research work. Moreover, Dr. Muhammad Khalid gratefully acknowledges the financial support of HEC Pakistan (project no. 20-14703/NRPU/R&D/HEC/2021). The authors are also thankful for the cooperation and collaboration of A.A.C.B from IQ-USP, Brazil, especially for his continuous support and providing computational lab facilities.

■ REFERENCES

(1) Shelton, D. P.; David, P.; Rice, J. E. Measurements and calculations of the hyperpolarizabilities of atoms and small molecules in the gas phase. *Chem. Rev.* **1994**, *94*, 3−29.

(2) Coe, B. J.; Foxon, S. P.; Harper, E. C.; Raftery, J.; Shaw, R.; Swanson, C. A.; Asselberghs, I.; Clays, K.; Brunschwig, B. S.; Fitch, A. G. Nonlinear optical and related properties of iron (II) pentacyanide complexes with quaternary nitrogen electron acceptor units. *Inorg. Chem.* **2009**, *48*, 1370−1379.

(3) Janjua, M. R. S. A.; Liu, C.-G.; Guan, W.; Zhuang, J.; Muhammad, S.; Yan, L.-K.; Su, Z.-M. Prediction of remarkably large second-order nonlinear optical properties of organoimido-substituted hexamolybdates. *J. Mater. Chem. A* **2009**, *113*, 3576−3587.

(4) Muhammad, S.; Xu, H.; Liao, Y.; Kan, Y.; Su, Z. Quantum mechanical design and structure of the Li@ B10H14 basket with a remarkably enhanced electro-optical response. *J. Am. Chem. Soc.* **2009**, *131*, 11833−11840.

(5) Marder, S. R.; Gorman, C. B.; Meyers, F.; Perry, J. W.; Bourhill, G.; Brédas, J.-L.; Pierce, B. M. A unified description of linear and nonlinear polarization in organic polymethine dyes. *Science* **1994**, *265*, 632−635.

(6) Blanchard-Desce, M.; Alain, V.; Bedworth, P. V.; Marder, S. R.; Fort, A.; Runser, C.; Barzoukas, M.; Lebus, S.; Wortmann, R. Large quadratic hyperpolarizabilities with donor−acceptor polyenes exhibiting optimum bond length alternation: correlation between structure and hyperpolarizability. *Chem.—Eur. J.* **1997**, *3*, 1091−1104.

(7) Yang, J.-S.; Liau, K.-L.; Li, C.-Y.; Chen, M.-Y. Meta conjugation effect on the torsional motion of aminostilbenes in the photoinduced intramolecular charge-transfer state. *J. Am. Chem. Soc.* **2007**, *129*, 13183−13192.

(8) Zyss, J.; Ledoux, I. Nonlinear optics in multipolar media: theory and experiments. *Chem. Rev.* **1994**, *94*, 77−105.

(9) Lee, S. H.; Park, J. R.; Jeong, M. Y.; Kim, H. M.; Li, S.; Song, J.; Ham, S.; Jeon, S. J.; Cho, B. R. First hyperpolarizabilities of 1, 3, 5-tricyanobenzene derivatives: origin of larger β values for the octupoles than for the dipoles. *ChemPhysChem* **2006**, *7*, 206−212.
(10) Lee, M. J.; Piao, M.; Jeong, M.-Y.; Hae Lee, S.; Min Kang, K.; Jeon, S.-J.; Gun Lim, T.; Rae Cho, B. Novel azo octupoles with large first hyperpolarizabilities. *J. Mater. Chem.* **2003**, *13*, 1030−1037.
(11) Meyers, F.; Marder, S.; Pierce, B.; Brédas, J. Tuning of large second hyperpolarizabilities in organic conjugated compounds. *Chem. Phys. Lett.* **1994**, *228*, 171−176.
(12) Coe, B. J.; Jones, L. A.; Harris, J. A.; Brunschwig, B. S.; Asselberghs, I.; Clays, K.; Persoons, A. Highly unusual effects of π-conjugation extension on the molecular linear and quadratic nonlinear optical properties of ruthenium (II) ammine complexes. *J. Am. Chem. Soc.* **2003**, *125*, 862−863.
(13) (a) Bella, S. D. Second-order nonlinear optical properties of transition metal complexes. *Chem. Soc. Rev.* **2001**, *30*, 355−366. (b) Coe, B. J. Switchable nonlinear optical metallochromophores with pyridinium electron acceptor groups. *Acc. Chem. Res.* **2006**, *39*, 383−393. (c) Kanis, D. R.; Ratner, M. A.; Marks, T. J. Design and construction of molecular assemblies with large second-order optical nonlinearities. Quantum chemical aspects. *Chem. Rev.* **1994**, *94*, 195−242.
(14) Ironside, C. N. Optical nonlinear effects in semiconductors. *Principles and Applications of Nonlinear Optical Materials*; Springer, 1993; pp 35−75.
(15) Wang, Q.; Yang, F.; Wang, X.; Zhou, J.; Ju, J.; Huang, L.; Gao, D.; Bi, J.; Zou, G. Deep-ultraviolet mixed-alkali-metal borates with induced enlarged birefringence derived from the structure rearrangement of the LiB3O5. *Inorg. Chem.* **2019**, *58*, 5949−5955.
(16) Mei, D.; Yin, W.; Feng, K.; Lin, Z.; Bai, L.; Yao, J. WuLiGaGe2Se6: A new IR nonlinear optical material with low melting point. *Inorg. Chem.* **2012**, *51*, 1035−1040.
(17) (a) Mao, F. F.; Hu, C. L.; Xu, X.; Yan, D.; Yang, B. P.; Mao, J. G. Bi (IO3) F2: the first metal iodate fluoride with a very strong second harmonic generation effect. *Angew. Chem.* **2017**, *129*, 2183−2187. (b) Chen, J.; Hu, C.-L.; Mao, F.-F.; Zhang, X.-H.; Yang, B.-P.; Mao, J.-G. LiMg (IO 3) 3: an excellent SHG material designed by single-site aliovalent substitution. *Chem. Sci.* **2019**, *10*, 10870−10875. (c) Zou, G.; Lin, C.; Jo, H.; Nam, G.; You, T. S.; Ok, K. M. Pb2BO3Cl: a tailor-made polar lead borate chloride with very strong second harmonic generation. *Angew. Chem.* **2016**, *128*, 12257−12261.
(18) You, F.; Liang, F.; Huang, Q.; Hu, Z.; Wu, Y.; Lin, Z. Pb2GaF2 (SeO3) 2Cl: band engineering strategy by aliovalent substitution for enlarging bandgap while keeping strong second harmonic generation response. *J. Am. Chem. Soc.* **2018**, *141*, 748−752.
(19) (a) Judeinstein, P.; Sanchez, C. Hybrid organic−inorganic materials: a land of multidisciplinarity. *J. Mater. Chem.* **1996**, *6*, 511−525. (b) Muhammad, S.; Xu, H.; Su, Z.; Fukuda, K.; Kishi, R.; Shigeta, Y.; Nakano, M. A new type of organic−inorganic hybrid NLO-phore with large off-diagonal first hyperpolarizability tensors: a two-dimensional approach. *Dalton Trans.* **2013**, *42*, 15053−15062. (c) Muhammad, S.; Minami, T.; Fukui, H.; Yoneda, K.; Kishi, R.; Shigeta, Y.; Nakano, M. Halide ion complexes of decaborane (B10H14) and their derivatives: noncovalent charge transfer effect on second-order nonlinear optical properties. *J. Mater. Chem. A* **2012**, *116*, 1417−1424.
(20) Terenziani, F.; Katan, C.; Badaeva, E.; Tretiak, S.; Blanchard-Desce, M. Enhanced two-photon absorption of organic chromophores: theoretical and experimental assessments. *Adv. Mater.* **2008**, *20*, 4641−4678.
(21) Liu, Z.-Q.; Fang, Q.; Cao, D.-X.; Wang, D.; Xu, G.-B. Triaryl boron-based A-π-A vs triaryl nitrogen-based D-π-D quadrupolar compounds for single-and two-photon excited fluorescence. *Org. Lett.* **2004**, *6*, 2933−2936.
(22) Verbiest, T.; Houbrechts, S.; Kauranen, M.; Clays, K.; Persoons, A. Second-order nonlinear optical materials: recent advances in chromophore design. *J. Mater. Chem.* **1997**, *7*, 2175−2189.
(23) Fernandes, S. S. M.; Belsley, M.; Pereira, A. I.; Ivanou, D.; Mendes, A. l.; Justino, L. L.; Burrows, H. D.; Raposo, M. M. M. Push−pull N, N-diphenylhydrazones bearing bithiophene or thienothiophene spacers as nonlinear optical second harmonic generators and as photosensitizers for nanocrystalline TiO2 dye-sensitized solar cells. *ACS Omega* **2018**, *3*, 12893−12904.
(24) Xu, H.; Zhang, M.; Zhang, A.; Deng, G.; Si, P.; Huang, H.; Peng, C.; Fu, M.; Liu, J.; Qiu, L. Novel second-order nonlinear optical chromophores containing multi-heteroatoms in donor moiety: design, synthesis, DFT studies and electro-optic activities. *Dyes Pigm.* **2014**, *102*, 142−149.
(25) Chandra, S.; Parmar, S.; Kumar, Y. Synthesis, spectroscopic, and antimicrobial studies on bivalent zinc and mercury complexes of 2-formylpyridine thiosemicarbazone. *Bioinorg. Chem. Appl.* **2009**, *2009*, 851316.
(26) Naseem, S.; Khalid, M.; Tahir, M. N.; Halim, M. A.; Braga, A. A.; Naseer, M. M.; Shafiq, Z. Synthesis, structural, DFT studies, docking and antibacterial activity of a xanthene based hydrazone ligand. *J. Mol. Struct.* **2017**, *1143*, 235−244.
(27) Tahir, M. N.; Khalid, M.; Islam, A.; Mashhadi, S. M. A.; Braga, A. A. Facile synthesis, single crystal analysis, and computational studies of sulfanilamide derivatives. *J. Mol. Struct.* **2017**, *1127*, 766−776.
(28) Jawaria, R.; Hussain, M.; Khalid, M.; Khan, M. U.; Tahir, M. N.; Naseer, M. M.; Braga, A. A. C.; Shafiq, Z. Synthesis, crystal structure analysis, spectral characterization and nonlinear optical exploration of potent thiosemicarbazones based compounds: A DFT refine experimental study. *Inorg. Chim. Acta* **2019**, *486*, 162−171.
(29) Subashchandrabose, S.; Krishnan, A. R.; Saleem, H.; Parameswari, R.; Sundaraganesan, N.; Thanikachalam, V.; Manikandan, G. Vibrational spectroscopic study and NBO analysis on bis (4-amino-5-mercapto-1, 2, 4-triazol-3-yl) methane using DFT method. *Spectrochim. Acta, Part A* **2010**, *77*, 877−884.
(30) James, C.; Raj, A. A.; Reghunathan, R.; Jayakumar, V.; Joe, I. H. Structural conformation and vibrational spectroscopic studies of 2, 6-bis (p-N, N-dimethyl benzylidene) cyclohexanone using density functional theory. *J. Raman Spectrosc.* **2006**, *37*, 1381−1392.
(31) Liu, J.-n.; Chen, Z.-r.; Yuan, S.-F. Study on the prediction of visible absorption maxima of azobenzene compounds. *J. Zhejiang Univ., Sci., B* **2005**, *6*, 584−589.
(32) Mulliken, R. S. Electronic population analysis on LCAO−MO molecular wave functions. II. overlap populations, bond orders, and covalent bond energies. *J. Chem. Phys.* **1955**, *23*, 1841−1846.
(33) Parr, R. G.; Pearson, R. G. Absolute hardness: companion parameter to absolute electronegativity. *J. Am. Chem. Soc.* **1983**, *105*, 7512−7516.
(34) Murray, J. S.; Politzer, P. Molecular electrostatic potentials and noncovalent interactions. *Wiley Interdiscip. Rev.: Comput. Mol. Sci.* **2017**, *7*, No. e1326.
(35) Luque, F.; López, J.; Orozco, M. Electrostatic interactions of a solute with a continuum. A direct utilization of ab initio molecular potentials for the prevision of solvent effects. *Theor. Chem. Acc.* **2000**, *103*, 343−345.
(36) Ali, A.; Khalid, M.; Tahir, M. N.; Imran, M.; Ashfaq, M.; Hussain, R.; Assiri, M. A.; Khan, I. Synthesis of diaminopyrimidine sulfonate derivatives and exploration of their structural and quantum chemical insights via SC-XRD and the DFT approach. *ACS Omega* **2021**, *6*, 7047−7057.
(37) Mahalakshmi, G.; Balachandran, V. NBO HOMO LUMO analysis and vibrational spectra (FTIR and FT Raman) of 1-Amino 4-methylpiperazine using ab initio HF and DFT methods. *Spectrochim. Acta, Part A* **2015**, *135*, 321−334.
(38) Arshad, M. N.; Al-Dies, A.-A. M.; Asiri, A. M.; Khalid, M.; Birinji, A. S.; Al-Amry, K. A.; Braga, A. A. Synthesis, crystal structures, spectroscopic and nonlinear optical properties of chalcone derivatives: a combined experimental and theoretical study. *J. Mol. Struct.* **2017**, *1141*, 142−156.
(39) Srnec, M.; Solomon, E. I. Frontier molecular orbital contributions to chlorination versus hydroxylation selectivity in the

https://doi.org/10.1021/acsomega.3c00421
ACS Omega 2023, 8, 13982−13992

non-heme iron halogenase SyrB2. *J. Am. Chem. Soc.* **2017**, *139*, 2396−2407.
(40) Mahmood, A.; Abdullah, M. I.; Nazar, M. F. Quantum chemical designing of novel organic non-linear optical compounds. *Bull. Korean Chem. Soc.* **2014**, *35*, 1391−1396.
(41) Amiri, S. S.; Makarem, S.; Ahmar, H.; Ashenagar, S. Theoretical studies and spectroscopic characterization of novel 4-methyl-5-((5-phenyl-1, 3, 4-oxadiazol-2-yl) thio) benzene-1, 2-diol. *J. Mol. Struct.* **2016**, *1119*, 18−24.
(42) Lesar, A.; Milošev, I. Density functional study of the corrosion inhibition properties of 1, 2, 4-triazole and its amino derivatives. *Chem. Phys. Lett.* **2009**, *483*, 198−203.
(43) Parr, R. G.; Donnelly, R. A.; Levy, M.; Palke, W. E. Electronegativity: the density functional viewpoint. *J. Chem. Phys.* **1978**, *68*, 3801−3807.
(44) Lawal, M. M.; Govender, T.; Maguire, G. E.; Kruger, H. G.; Honarparvar, B. DFT study of the acid-catalyzed esterification reaction mechanism of methanol with carboxylic acid and its halide derivatives. *Int. J. Quantum Chem.* **2018**, *118*, No. e25497.
(45) (a) Pearson, R. G. Absolute electronegativity and hardness correlated with molecular orbital theory. *Proc. Natl. Acad. Sci.* **1986**, *83*, 8440−8441. (b) Koopmans, T. The classification of wave functions and eigen-values to the single electrons of an atom. *Physica* **1934**, *1*, 104−113.
(46) Li, Z. a.; Kim, H.; Chi, S.-H.; Hales, J. M.; Jang, S.-H.; Perry, J. W.; Jen, A. K.-Y. Effects of counterions with multiple charges on the linear and nonlinear optical properties of polymethine salts. *Chem. Mater.* **2016**, *28*, 3115−3121.
(47) Papadopoulos, M. G.; Sadlej, A. J.; Leszczynski, J. *Non-Linear Optical Properties of Matter*; Springer, 2006. DOI: 10.1007/1-4020-4850-5.
(48) (a) Crasta, V.; Ravindrachary, V.; Bhajantri, R.; Gonsalves, R. Growth and characterization of an organic NLO crystal: 1-(4-methylphenyl)-3-(4-methoxyphenyl)-2-propen-1-one. *J. Cryst. Growth* **2004**, *267*, 129−133. (b) Mahmood, A.; Abdullah, M. I.; Khan, S. U.-D. Enhancement of nonlinear optical (NLO) properties of indigo through modification of auxiliary donor, donor and acceptor. *Spectrochim. Acta, Part A* **2015**, *139*, 425−430. (c) Khalid, M.; Khan, M. U.; Shafiq, I.; Hussain, R.; Mahmood, K.; Hussain, A.; Jawaria, R.; Hussain, A.; Imran, M.; Assiri, M. A.; et al. NLO potential exploration for D−π−A heterocyclic organic compounds by incorporation of various π-linkers and acceptor units. *Arabian J. Chem.* **2021**, *14*, 103295.
(49) Khan, M. U.; Khalid, M.; Ibrahim, M.; Braga, A. A. C.; Safdar, M.; Al-Saadi, A. A.; Janjua, M. R. S. A. First theoretical framework of triphenylamine−dicyanovinylene-based nonlinear optical dyes: structural modification of π-linkers. *J. Phys. Chem. C* **2018**, *122*, 4009−4018.
(50) Khan, M. U.; Ibrahim, M.; Khalid, M.; Jamil, S.; Al-Saadi, A. A.; Janjua, M. R. S. A. Quantum chemical designing of indolo [3, 2, 1-jk] carbazole-based dyes for highly efficient nonlinear optical properties. *Chem. Phys. Lett.* **2019**, *719*, 59−66.
(51) Khan, M. U.; Ibrahim, M.; Khalid, M.; Braga, A. A. C.; Ahmed, S.; Sultan, A. Prediction of second-order nonlinear optical properties of D−π−A compounds containing novel fluorene derivatives: a promising route to giant hyperpolarizabilities. *J. Cluster Sci.* **2019**, *30*, 415−430.
(52) Muhammad, S.; Kumar, S.; Koh, J.; Saravanabhavan, M.; Ayub, K.; Chaudhary, M. Synthesis, characterisation, optical and nonlinear optical properties of thiazole and benzothiazole derivatives: a dual approach. *Mol. Simul.* **2018**, *44*, 1191−1199.
(53) Mendis, B. S.; De Silva, K. N. A comprehensive study of linear and non-linear optical properties of novel charge transfer molecular systems. *J. Mol. Struct.: THEOCHEM* **2004**, *678*, 31−38.
(54) Kara Zaitri, L.; Mekelleche, S. M. Computational study of linear and nonlinear optical properties of substituted thiophene imino dyes using long-range corrected hybrid DFT methods. *Mol. Phys.* **2020**, *118*, 1618508.
(55) Alparone, A. Linear and nonlinear optical properties of nucleic acid bases. *Chem. Phys.* **2013**, *410*, 90−98.
(56) Plaquet, A.; Guillaume, M.; Champagne, B.; Castet, F.; Ducasse, L.; Pozzo, J.-L.; Rodriguez, V. In silico optimization of merocyanine-spiropyran compounds as second-order nonlinear optical molecular switches. *Phys. Chem. Chem. Phys.* **2008**, *10*, 6223−6232.
(57) Muhammad, S.; Shehzad, R. A.; Iqbal, J.; Al-Sehemi, A. G.; Saravanabhavan, M.; Khalid, M. Benchmark study of the linear and nonlinear optical polarizabilities in proto-type NLO molecule of para-nitroaniline. *J. Theor. Comput. Chem.* **2019**, *18*, 1950030.
(58) Loukova, G. V.; Milov, A. A.; Vasiliev, V. P.; Minkin, V. I. Modeling of the spatial and electronic structure and the dipole moment of titanocene dicarboranyl. *Russ. Chem. Bull.* **2020**, *69*, 218−228.
(59) Poirier, R.; Kari, R.; Csizmadia, I. G. *Handbook of Gaussian Basis Sets*; Elsevier Science Publishers, 1985.
(60) Burke, K.; Werschnik, J.; Gross, E. K. U. Time-dependent density functional theory: Past, present, and future. *J. Chem. Phys.* **2005**, *123*, 062206.
(61) Hanwell, M. D.; Curtis, D. E.; Lonie, D. C.; Vandermeersch, T.; Zurek, E.; Hutchison, G. R. Avogadro: an advanced semantic chemical editor, visualization, and analysis platform. *J. Cheminf.* **2012**, *4*, 17.
(62) Dennington, R.; Keith, T. A.; Millam, J. M. *GaussView 6.0. 16*; Semichem Inc.: Shawnee Mission, KS, USA, 2016.
(63) Sakthivel, S.; Alagesan, T.; Muthu, S.; Abraham, C. S.; Geetha, E. Quantum mechanical, spectroscopic study (FT-IR and FT-Raman), NBO analysis, HOMO-LUMO, first order hyperpolarizability and docking studies of a non-steroidal anti-inflammatory compound. *J. Mol. Struct.* **2018**, *1156*, 645−656.
(64) O'boyle, N. M.; Tenderholt, A. L.; Langner, K. M. Cclib: a library for package-independent computational chemistry algorithms. *J. Comput. Chem.* **2008**, *29*, 839−845.

https://doi.org/10.1021/acsomega.3c00421
ACS Omega 2023, 8, 13982−13992